THE JOURNAL OF PHYSICAL CHEMISTRY C

Article

pubs.acs.org/JPCC

Geometric and Electronic Structure of Templated C_{60} on Diindenoperylene Thin Films

A. Hinderhofer,*[,†,‡] A. Gerlach,[†] K. Broch,[†] T. Hosokai,[¶] K. Yonezawa,[‡] K. Kato,[‡] S. Kera,[‡] N. Ueno,[‡] and F. Schreiber[†]

[†]Institute for Applied Physics, University of Tübingen, Auf der Morgenstelle 10, 72076 Tübingen, Germany

[‡]Graduate School of Advanced Integration Science, Chiba University, 1-33 Yayoi-cho, Inage-ku, Chiba 263-8522, Japan

[¶]Department of Materials and Science, Iwate University, Ueda 4-3-5, Morioka, Iwate 020-8551, Japan

ABSTRACT: The structural order of C_{60} thin films is shown to be significantly improved by inserting a templating layer of diindenoperylene (DIP) between the SiO_2 substrate and C_{60}. In contrast to growth on an amorphous substrate like SiO_2, C_{60} grown on DIP exhibits alignment of *fcc*-domains with the (111) plane parallel to the substrate and a significant increase of the coherent in-plane island size by a factor of ~4. Modification of the structural quality of the DIP bottom layer leads to a change in structural order in the C_{60} top layer. In addition, ultraviolet photoelectron spectroscopy data from templated and nontemplated C_{60} films are discussed. In contrast to other anisotropic organic molecules, for C_{60} the spectral broadening and density of states of the highest occupied molecular orbital region do not depend significantly on the structural order in the C_{60} film, which can be rationalized by the isotropic shape of the C_{60} molecule.

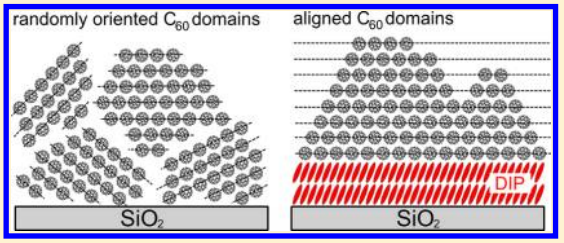

INTRODUCTION

For growth of organic thin films the structure and morphology depends strongly on the substrate onto which they are deposited.[1,2] This was demonstrated, for example, by the surface modification of an inorganic substrate with an organic self-assembled monolayer (SAM), which influenced the resulting growth behavior.[3−10] For such heterostructures the growth behavior of the top layer is mostly discussed in terms of surface energies, although also some degree of azimuthal alignment has been observed.[10] In contrast, a close relationship between two organic layers can be observed in organic−organic heteroepitaxy.[11−15] There, the growth behavior of the deposited compound depends on the, usually anisotropic, potential surface of both involved materials. The control of the top layer morphology by tuning of the bottom layer was also discussed as templating, particularly for changing the molecular orientation relative to the surface (standing orientation vs lying orientation).[16,17]

The structural relationship at an organic−organic heterointerface resulting from the nonequilibrium growth process has a large impact on electrical properties, inter alia charge carrier generation, and transport.[18,19] For example, for organic field effect transistors it was shown that an organic templating layer may improve the electronic mobility of the active material substantially.[14,20−22] In this regard, an important point for small-molecule organic semiconductors can be the orientation of the molecules. Frequently, there is at least a competition between lying down and standing up orientation,[6,23] which depends strongly on the underlying substrate. Other systems, such as PTCDA, exhibit a very strong tendency to form lying-down structures, almost independent of the substrate.[10,24−27] In this context, C_{60} is a rather unique case in the area of small-molecule organic semiconductors, since it exhibits essentially rotational symmetry. The issue of lying-down vs standing-up orientation does not complicate matters, and the orientational degrees of freedom in structure formation enter basically only via the orientation of the lattice planes and their distribution or alignment. C_{60} was shown to grow with low structural order on several inorganic substrates like SiO_2,[28] quartz glass,[29] and sapphire[20] but crystallizes well on organics like pentacene[20,30] or sexiphenyl.[31,32]

In this paper we study the influence of a diindenoperylene (DIP, Figure 1) templating layer[33−37] on the growth and electronic structure of C_{60}. The combination of C_{60} and DIP in a heterostructure was shown to exhibit excellent photovoltaic performance,[38,39] which is related to the high exciton diffusion length in DIP[40,41] and the favorable energy level alignment of both materials.[38,42,43] In addition, we investigate to which extent structural properties like roughness, domain size, and

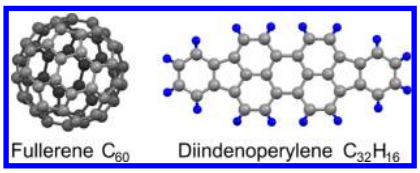

Figure 1. Sketch of fullerene (C_{60}) and diindenoperylene (DIP, $C_{32}H_{16}$).

Received: October 26, 2012
Revised: November 27, 2012
Published: November 27, 2012

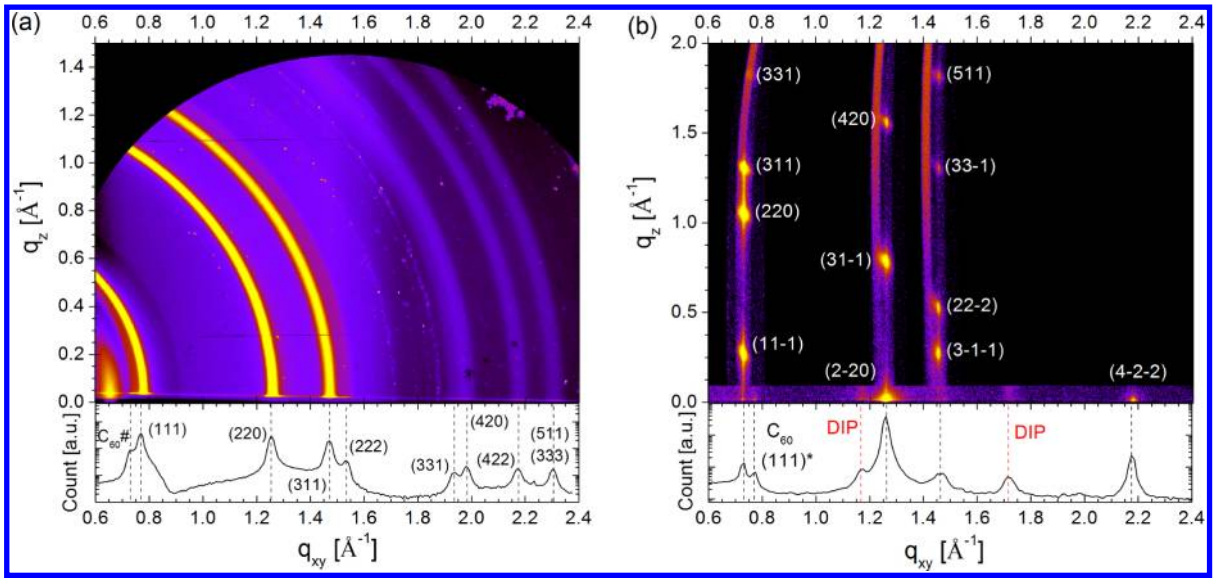

Figure 2. (a) Reciprocal space map from a 60 nm C_{60} film recorded with a MARCCD area detector. At the bottom additional GIXD data measured with a point detector at q_z = 0.02 Å^{-1} are shown. (b) 2-Dimensional GIXD data from a 15 nm C_{60} film grown on a DIP templating layer (d = 4 nm) indexed according to the C_{60} *fcc* structure. The data consist of four detector scans at a fixed angle of incidence at 0.1° performed with a PILATUS II area detector. Images from each data point were transformed into q coordinates and then assembled into one image. One scan was performed parallel to the substrate plane, for which at the bottom the integrated GIXD data are shown. Three scans were performed along the C_{60} crystal truncation rods.

crystallinity of the DIP templating layer influence the growth of C_{60}.

EXPERIMENTAL SECTION

Organic thin films were deposited on silicon wafers with native SiO_2 (surface roughness σ_{rms} = 0.3 nm) under ultra high vacuum (UHV) conditions (base pressure <6 × 10^{-7} Pa) by thermal evaporation. Before deposition, substrates were cleaned ultrasonically with acetone, isopropyl alcohol, and ultra pure water, followed by heating to 700 K in the UHV growth chamber. The growth rate was between 0.1 and 0.3 nm/min monitored by in situ X-ray reflectivity (XRR) and a quartz crystal microbalance. All C_{60} films were deposited at a substrate temperature of T = 300 K. The substrate temperature for DIP deposition was varied between T = 200 and 380 K with resistive heating and nitrogen cooling. Data acquisition, ultraviolet photoelectron spectroscopy (UPS), and X-ray scattering were performed at T = 300 K.

In situ XRR and grazing incidence X-ray diffraction (GIXD) were performed at the X04SA beamline of the Swiss Light Source, Paul Scherrer Institut, Villigen, Switzerland (λ = 0.10 nm). One additional 2-dimensional GIXD scan shown in Figure 2a was measured with a MARCCD area detector at beamline ID10B[44] (λ = 0.092 nm) of the ESRF in Grenoble, France. Modeling of XRR data was done with Motofit.[45] Peak indexing of DIP is based on the crystal structure (P21/a polymorph) reported in ref 35. Lower limits of the in-plane coherent crystal sizes l_s were determined by the Scherrer formula $l_s = (\text{fwhm})^{-1} \times 0.9394 \times K_s$, where K_s = 1.0747 is the Scherrer constant for spherical grains and fwhm is the full-width half-maximum of the peak (in Å^{-1}) determined with a Gaussian fit-function.[46] The instrumental broadening of the diffractometer was not included in the calculation, therefore only lower limits of l_s are given.

He I UPS experiments were performed with a home-built UHV system[47] equipped with a PHOIBOS-HSA100 analyzer with an energy resolution of 60 meV and an acceptance angle of ±9°. UPS were measured at a light incident angle of 45° and an electron emission angle of 0° (normal emission). After growth in a UHV preparation chamber the samples were directly transferred to the measurement chamber without breaking the vacuum. The vacuum level (VL) was obtained by applying a sample bias of −5 V during the UPS measurements.

RESULTS

X-ray Scattering. To study the structure of C_{60} thin films we compare first a reciprocal space map of a C_{60} film grown on SiO_2 (C_{60}/SiO_2; Figure 2a) with data from C_{60} grown on DIP (C_{60}/DIP; Figure 2b). The C_{60}/SiO_2 film exhibits broad diffraction rings indicating crystalline domains without preferred orientation. Indexing is done according to the C_{60} *fcc* structure reported in ref 48. One reflection, indexed as C_{60}# in the bottom GIXD data, does not stem from the C_{60} *fcc* structure. Its q-value (q = 0.725 Å^{-1}) coincides with the (100) reflection from the C_{60} *hcp* structure. This observation is in agreement with single crystal growth, where a small fraction of crystals adopt *hcp* packing.[48] Note that in the indexing of GIXD data at the bottom of Figure 2a only one index for each reflection is given, since other reflections with the same $|q|$ cannot be distinguished. The scattering data of the C_{60}/SiO_2 film shown here are in agreement with data presented in ref 28.

Figure 2b displays 2-dimensional GIXD data from a C_{60}/DIP heterostructure. At the bottom the integrated GIXD intensity is shown. Indexing is done again according to the C_{60} *fcc* structure. Compared to C_{60} grown on SiO_2 (Figure 2a) the diffraction pattern of C_{60} grown on DIP shows significant differences. The distribution of Bragg reflections reveals the alignment of the *fcc*-(111) crystal plane parallel to the substrate. Only a small fraction of crystallites nucleates with a random orientation as indicated by the weak C_{60} (111)* index. Note that the Bragg reflection at q_{xy} = 0.725 Å^{-1} stems not from the *hcp* structure as in Figure 2a. Instead, this peak is the projection

dx.doi.org/10.1021/jp3106056 | J. Phys. Chem. C 2013, 117, 1053−1058

of the *fcc*-(11−1) Bragg reflection onto the q_{xy} plane. The width of the *fcc* Bragg reflections in q_z (out-of-plane) is relatively large because of the small crystal size in the q_z direction limited by the film thickness of 15 nm. The in-plane coherent crystal sizes l_s of both C_{60} films were determined with the Scherrer formula to be l_s = 7 nm for the C_{60}/SiO_2 film and l_s = 28 nm for the C_{60}/DIP film. For the determination of l_s of both C_{60} films we choose the (2−20) and (4−2−2) reflections and averaged over the obtained values. The difference in l_s is clear evidence for the improved crystal quality and reduction of crystal defect density in the C_{60}/DIP film compared to the C_{60}/SiO_2 film.

Complementary XRR data are shown in Figure 3. Here, the templated C_{60}/DIP film exhibits two pronounced Bragg

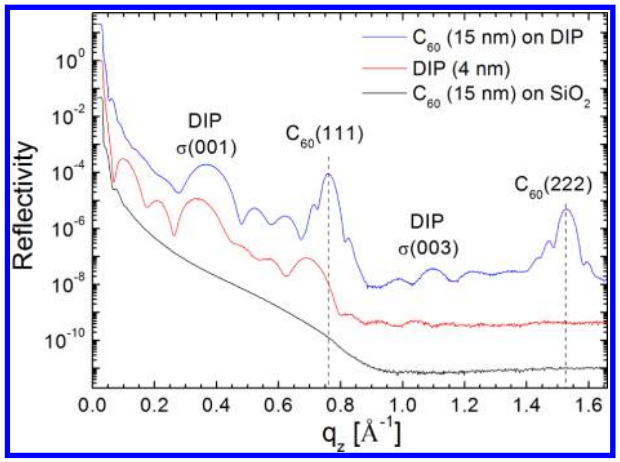

Figure 3. Specular X-ray reflectivity data from C_{60} films (d = 15 nm) grown on SiO_2 and DIP (d = 4 nm). XRR data of the thin DIP film before C_{60} deposition are shown for comparison.

reflections, indexed (111) and (222). However, no Bragg reflection is observed for the C_{60}/SiO_2 film. The root mean squared roughness (σ_{rms}) determined from the Kiessig-fringes near the total reflection edge is σ_{rms} = 3.0 ± 0.3 nm for both C_{60} films, indicating that the roughening in this thickness region (~15 nm) does not strongly depend on the templating effect. The XRR data confirm the enhanced crystal quality and orientational ordering of C_{60} on DIP in comparison to C_{60} grown on SiO_2.

Figure 4 summarizes the difference of the structure of the C_{60}/SiO_2 and C_{60}/DIP films. In the C_{60}/SiO_2 film grains are

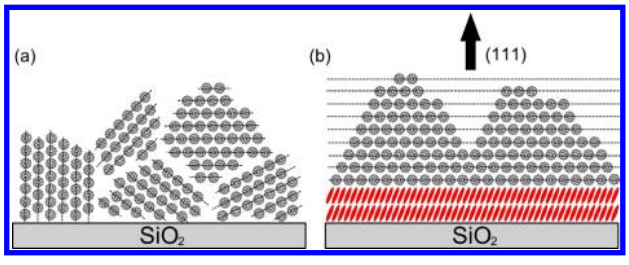

Figure 4. Sketch of domain orientations of C_{60} films grown on SiO_2 (a) and DIP (b).

small and have no preferred orientation. In contrast, coherently ordered domains in the C_{60}/DIP film are larger and oriented with the (111) plane parallel to the surface.

For a more detailed understanding of the observed templating effect we test if the structural quality or the roughness of the templating layer influences the C_{60} growth. The growth of DIP on SiO_2 is already well established for different thicknesses and temperatures.[34,36,49] DIP films are predominantly textured with the (001) plane (DIP HT phase) parallel to the substrate, which corresponds to roughly standing molecules. In the thickness region below ~10 nm, DIP exhibits layer-by-layer growth with a metastable DIP structure[36,50] followed by rapid roughening for thicker films.[34] Generally, films grown at elevated substrate temperatures are of higher crystal quality compared to low temperature deposited films.[17,49]

Figure 5a shows GIXD data of 15 nm C_{60} films grown on DIP films with different thicknesses and on bare SiO_2.

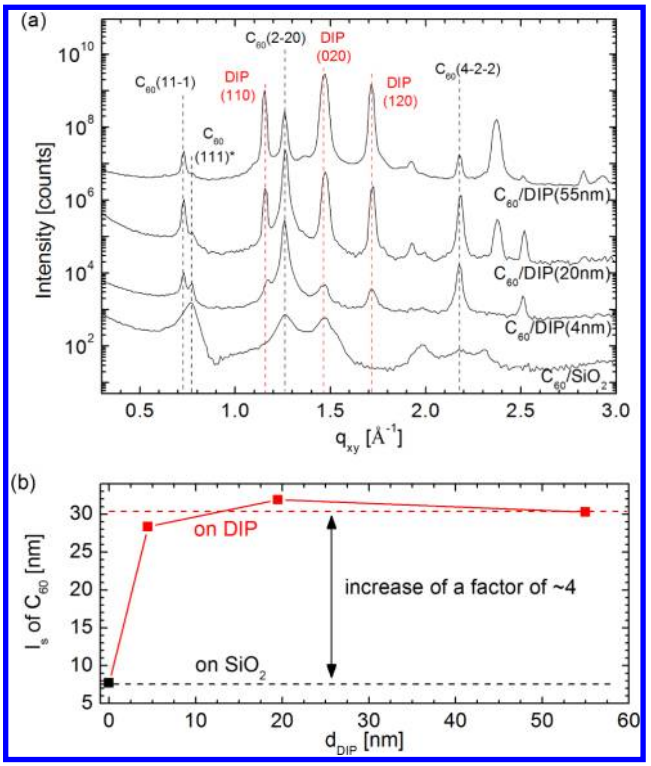

Figure 5. (a) GIXD of C_{60} ($d \approx$ 15 nm; T = 300 K) on DIP films (T = 380 K) with different thicknesses and on SiO_2. Curves are shifted for clarity. (b) In-plane coherent island size (l_s) of C_{60} determined from the GIXD data in part a. For the determination of l_s we averaged the obtained values from several Bragg reflections.

Thicknesses (d), σ_{rms}, and deposition temperatures (T) of the DIP templating layers are summarized in Table 1. Clearly the peak width and intensity of the C_{60} reflections vary for different DIP bottom layers. As an indicator for structural quality for the obtained films, we use the coherent in-plane island size (l_s) evaluated with the Scherrer formula. Figure 5b shows the correlation between l_s of the C_{60} film with the DIP film thickness. As already shown, the crystal quality of the C_{60} film is enhanced strongly (l_s increase by a factor of ~4) by already ~2−3 monolayers of DIP. For thicker templating layers the l_s of the C_{60} film is roughly constant for DIP thicknesses of at least up to 55 nm. We determined σ_{rms} of the three DIP templating layers (Table 1) from reflectivity data (not shown). The obtained roughness values are in agreement with the rapid roughening observed for DIP.[34] The increasing σ_{rms} for thick templating layers seem to have no effect on the C_{60} coherent in-

dx.doi.org/10.1021/jp3106056 | J. Phys. Chem. C 2013, 117, 1053−1058

plane island size, which stays nearly constant in the studied thickness region (Figure 5b).

To further examine if a decrease in crystallinity in the DIP bottom layer affects the crystal quality of the C_{60} film, we tuned the structure of the DIP templating layer by the substrate temperature during growth. Figure 6a shows GIXD data of 15 nm C_{60} films grown on DIP films ($d \approx 15$ nm) prepared at T = 200, 300, and 380 K. All three templating layers consist predominantly of textured DIP HT phase domains; however, l_s of DIP is significantly reduced at lower T, which was also demonstrated in refs 17 and 49. Figure 6b compares the l_s of C_{60} films with the l_s of the underlying DIP film. Increasing the l_s of the DIP templating layer results in a clear increase of the l_s of the C_{60} film. This observation implies that crystal defects of the substrate surface or templating material directly limit the crystal quality of the top layer. We note that in the applied scattering geometry, the X-ray beam probes the complete film and the derived l_s values are therefore an average in-plane coherent island size of the entire film. Since the coherent island size may be different at different thicknesses of a film, we compare only l_s values of films with a similar thickness. We conclude that defect free terraces of the templating material are needed for undisturbed C_{60} nucleation. Large-scale roughness does not appear to disturb the C_{60} templating significantly.

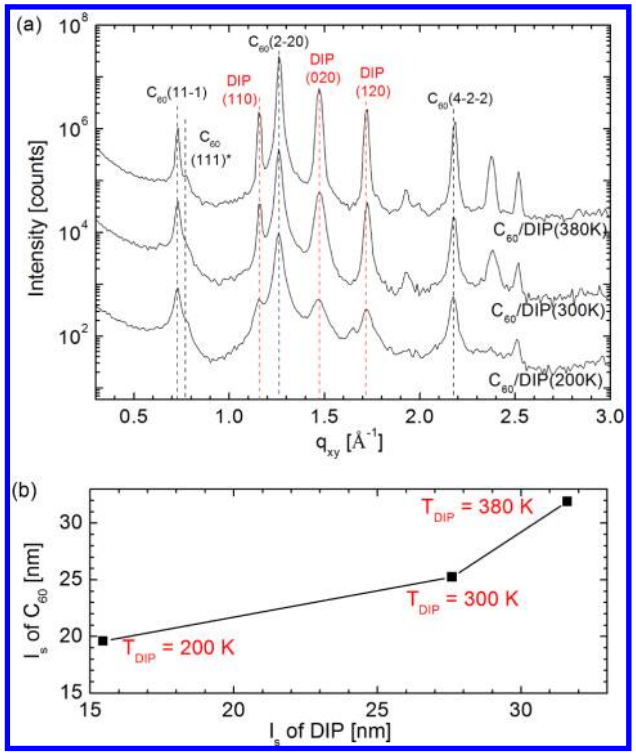

Figure 6. (a) GIXD of C_{60} ($d \approx 15$ nm; T = 300 K) on DIP films ($d \approx 15$ nm) prepared at T = 200, 300, and 380 K. Curves are shifted for clarity. (b) In-plane coherent island size (l_s) of C_{60} dependent on the l_s of the underlying DIP films determined from the GIXD data in part a. For the determination of l_s of DIP and C_{60} films we averaged the obtained values from several Bragg reflections.

UPS. Since C_{60}/DIP films are highly relevant for photovoltaic applications,[38] we study whether the templating effect demonstrated above influences the electronic structure of C_{60}.

Figure 7a shows UPS data of the highest occupied molecular orbital (HOMO) region of C_{60} grown on DIP and SiO_2. The overall shape of the HOMO and HOMO-1 states in Figure 7a corresponds to spectra measured for C_{60} thin films on various inorganic and organic substrates/films.[30,53−55] The similarity to the gas phase spectra of C_{60}[56] indicates only weak interaction between molecules in the thin film. Apart from a spectral shift of 150 meV, resulting from the different energy level alignment (ELA) of the C_{60} film to the DIP layer and the SiO_2 substrate, both spectra from the C_{60} films are essentially identical. This can be seen more clearly in the inset in Figure 7a, where the data are overlaid and the C_{60}/DIP data were shifted by 150 meV. In addition, also the ionization potentials (IP) determined by the secondary electron cutoff and the HOMO onset are equal (6.4 eV) for both C_{60} films. Strong changes in

Table 1. Thickness (d), Roughness (σ_{rms}), and Deposition Temperature (T) of DIP Templating Layers

d [nm]	σ_{rms} [nm]	T [K]
4.5	0.8	380
19.5	1.5	380
55	3.4	380

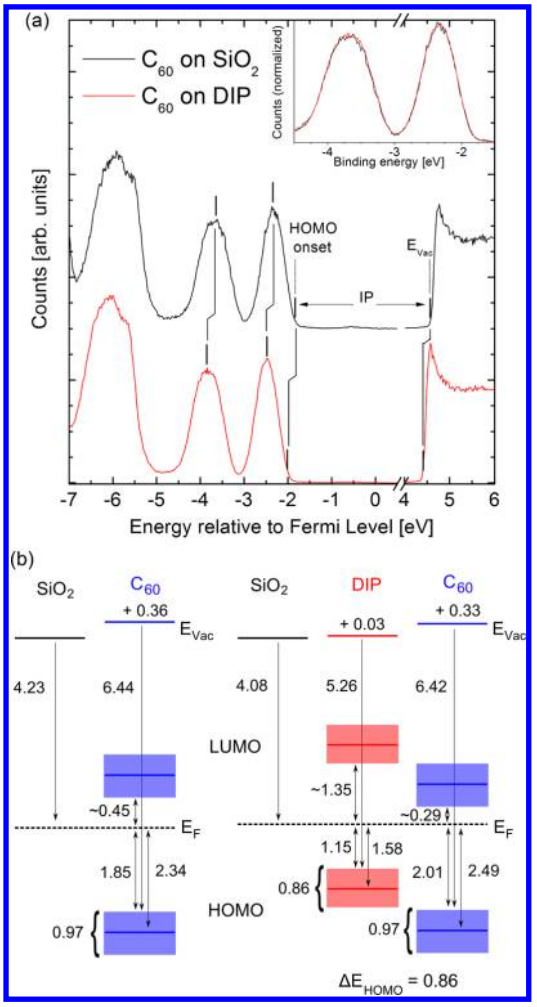

Figure 7. (a) UPS data from C_{60} (d = 13 nm) grown on SiO_2 and grown on DIP (d = 4 nm). The inset shows the normalized HOMO regions of both data sets with the C_{60}/DIP data shifted by 150 meV. (b) Sketch of the electronic level alignment from the UPS data in part a. LUMO levels were taken from refs 51 and 52. All values are given in eV and have an error bar of ±0.05 eV. The width of the HOMO state is determined by the respective onsets.

dx.doi.org/10.1021/jp3106056 | J. Phys. Chem. C 2013, 117, 1053−1058

structure and domain orientation for organic thin films lead to a significant change in spectral width of the HOMO or the IP depending on the molecular system.[57−59] However, our data demonstrate that at room temperature thin films of C_{60} do not show these effects because of the reasons described below.

In general several mechanisms may influence the HOMO bandwidth of a molecular material.[60,61] For instance, in a nonuniform or disordered film the polarization energy (final state effect) and the intermolecular interaction (initial state effect) are locally different, resulting in slightly different ionization energies at different positions and therefore in spectral broadening. Another broadening effect is associated with band dispersion due to delocalization of the electronic states, which can be observed only for large single crystals of C_{60}[62] and can therefore be omitted in the following discussion. In comparison to the C_{60}/SiO_2 film we may expect spectral sharpening for the C_{60}/DIP film, because of the improved crystal quality. The island size of the C_{60}/SiO_2 film is much smaller compared to that of the C_{60}/DIP film, implying that the density of crystal defects is higher in the C_{60}/SiO_2 film compared to the C_{60}-on-DIP film. However, the absence of any difference in the width of the C_{60} states implies that a small coherent island size in a C_{60} film has no significant impact on the polarization energy/intermolecular interaction. This observation may be rationalized by the high-symmetry shape of the single C_{60} molecule and its rotation at room temperature,[54,63] which results in a much smaller local polarization/interaction variation due to crystal defects in comparison to anisotropic rod-like molecules.

For the mechanisms of energy level alignment at the organic−inorganic and organic−organic interfaces several different models have been discussed[64−70] without a definitive conclusion in the literature. Figure 7b summarizes the ELA of two measured samples. For a low work function substrate like SiO_2 (WF = 4.23 eV) the C_{60} LUMO (lowest unoccupied molecular orbital) level is presumably located at the substrate Fermi level leading to an interface dipole of 0.36 eV. For organic−organic heterostructures the ELA of the top layer is typically governed by the energetic position of the bottom layer. The difference of the HOMO onsets of DIP and C_{60} as determined here is ΔE_{HOMO} = 0.86 eV, similar to values reported for a DIP/C_{60} heterostructure on PEDOT:PSS[38] and for the vice versa heterostructure (DIP-on-C_{60}).[43]

SUMMARY

In summary, we demonstrated that the structural order of C_{60} is significantly improved by inserting a DIP templating layer between the SiO_2 substrate and C_{60} film. In contrast to growth on an amorphous substrate like SiO_2, C_{60} grown on a DIP film exhibits alignment of *fcc* domains with the (111) plane parallel to the substrate and a significant increase of the coherent in-plane island size (l_s) by a factor of ∼4. In addition, it was shown that an increase in structural order of the DIP templating layer leads to a similar increase of structural order in the C_{60} top layer. UPS measurements revealed that the spectral broadening of the C_{60} HOMO region interestingly do not depend significantly on the structural order in the C_{60} film. This observation can be rationalized by the highly symmetric shape of the C_{60} molecule.

AUTHOR INFORMATION

Corresponding Author

*E-mail: alexander.hinderhofer@chiba-u.jp.

Notes

The authors declare no competing financial interest.

ACKNOWLEDGMENTS

The authors thank F. Bussolotti and S. Duhm for helpful discussions. We are grateful to S. Leake and P. Willmott at the MS beamline of the Swiss Light Source and A. Vorobiev at beamline ID10B of the European Synchrotron Radiation Facility (ESRF) whose great efforts have made these experiments possible. This research project has been supported by the DFG, the Global-COE program of MEXT (G03) at Chiba University, and the European Commission under the seventh Framework Programme: Research Infrastructures (Grant Agreement Number 226716). A.H. acknowledges support from the JSPS.

REFERENCES

(1) Witte, G.; Wöll, C. *J. Mater. Res.* **2004**, *19*, 1889−1916.
(2) Schreiber, F. *Phys. Status Solidi* **2004**, *201*, 1037.
(3) Käfer, D.; Ruppel, L.; Witte, G. *Phys. Rev. B* **2007**, *75*, 085309.
(4) Desai, T. V.; Woll, A. R.; Schreiber, F.; Engstrom, J. R. *J. Phys. Chem. C* **2010**, *114*, 20120−20129.
(5) Zhang, X. N.; Barrena, E.; de Oteyza, D. G.; Souza, E. D.; Dosch, H. *J. Appl. Phys.* **2008**, *104*, 104308.
(6) Desai, T. V.; Hong, S.; Woll, A. R.; Hughes, K. J.; Kaushik, A. P.; Clancy, P.; Engstrom, J. R. *J. Chem. Phys.* **2011**, *134*, 224702.
(7) Hayakawa, R.; Turak, A.; Zhang, X.; Hiroshiba, N.; Dosch, H.; Chikyow, T.; Wakayama, Y. *J. Chem. Phys.* **2010**, *133*, 034706.
(8) Zhu, H.; Li, Q. L.; She, X. J.; Wang, S. D. *Appl. Phys. Lett.* **2011**, *98*, 243304.
(9) Yang, H.; Shin, T. J.; Ling, M.-M.; Cho, K.; Ryu, C. Y.; Bao, Z. *J. Am. Chem. Soc.* **2005**, *127*, 11542−11543.
(10) Gerstenberg, M. C.; Schreiber, F.; Leung, T. Y. B.; Bracco, G.; Forrest, S. R.; Scoles, G. *Phys. Rev. B* **2000**, *61*, 7678−7685.
(11) Forrest, S. R. *Chem. Rev.* **1997**, *97*, 1793−1896.
(12) Sassella, A.; Campione, M.; Borghesi, A. *Riv. Nuovo Cimento Soc. Ital. Fis.* **2008**, *31*, 457.
(13) Raimondo, L.; Moret, M.; Campione, M.; Borghesi, A.; Sassella, A. *J. Phys. Chem. C* **2011**, *115*, 5880−5885.
(14) Yang, J.; Yan, D. *Chem. Soc. Rev.* **2009**, *38*, 2634−2645.
(15) Hinderhofer, A.; Schreiber, F. *ChemPhysChem* **2012**, *13*, 628−643.
(16) Sullivan, P.; Jones, T. S.; Ferguson, A. J.; Heutz, S. *Appl. Phys. Lett.* **2007**, *91*, 233114.
(17) Hinderhofer, A.; Hosokai, T.; Frank, C.; Novák, J.; Gerlach, A.; Schreiber, F. *J. Phys. Chem. C* **2011**, *115*, 16155−16160.
(18) Peumans, P.; Yakimov, A.; Forrest, S. R. *J. Appl. Phys.* **2003**, *93*, 3693−3723.
(19) Brütting, W.; Berleb, S.; Mückl, A. G. *Org. Electron.* **2001**, *2*, 1−36.
(20) Itaka, K.; Yamashiro, M.; Yamaguchi, J.; Haemori, M.; Yaginuma, S.; Matsumoto, Y.; Kondo, M.; Koinuma, H. *Adv. Mater.* **2006**, *18*, 1713−1716.
(21) Kraus, M.; Richler, S.; Opitz, A.; Brütting, W.; Haas, S.; Hasegawa, T.; Hinderhofer, A.; Schreiber, F. *J. Appl. Phys.* **2010**, *107*, 094503.
(22) Haemori, M.; Yamaguchi, J.; Yaginuma, S.; Itaka, K.; Koinuma, H. *Jpn. J. Appl. Phys.* **2005**, *44*, 3740−3742.
(23) Dürr, A. C.; Koch, N.; Kelsch, M.; Ruehm, A.; Ghijsen, J.; Johnson, R. L.; Pireaux, J.-J.; Schwartz, J.; Schreiber, F.; Dosch, H.; Kahn, A. *Phys. Rev. B* **2003**, *68*, 115428.
(24) Fenter, P.; Schreiber, F.; Zhou, L.; Eisenberger, P.; Forrest, S. R. *Phys. Rev. B* **1997**, *56*, 3046−3053.
(25) Hooks, D. E.; Fritz, T.; Ward, M. D. *Adv. Mater.* **2001**, *13*, 227−241.
(26) Krause, B.; Schreiber, F.; Dosch, H.; Pimpinelli, A.; Seeck, O. H. *Europhys. Lett.* **2004**, *65*, 372.

(27) Kilian, L.; Hauschild, A.; Temirov, R.; Soubatch, S.; Schöll, A.; Bendounan, A.; Reinert, F.; Lee, T.-L.; Tautz, F. S.; Sokolowski, M.; Umbach, E. *Phys. Rev. Lett.* **2008**, *100*, 136103.
(28) Singh, T. B.; Sariciftci, N. S.; Yang, H.; Yang, L.; Plochberger, B.; Sitter, H. *Appl. Phys. Lett.* **2007**, *90*, 213512.
(29) Yim, S.; Jones, T. S. *Appl. Phys. Lett.* **2009**, *94*, 021911.
(30) Salzmann, I.; Duhm, S.; Opitz, R.; Johnson, R. L.; Rabe, J. P.; Koch, N. *J. Appl. Phys.* **2008**, *104*, 114518.
(31) Chen, W.; Zhang, H.; Huang, H.; Chen, L.; Wee, A. T. S. *ACS Nano* **2008**, *2*, 693−698.
(32) Zhong, J. Q.; Huang, H.; Mao, H. Y.; Wang, R.; Zhong, S.; Chen, W. *J. Chem. Phys.* **2011**, *134*, 154706.
(33) Heinemeyer, U.; Scholz, R.; Gisslén, L.; Alonso, M. I.; Ossó, J. O.; Garriga, M.; Hinderhofer, A.; Kytka, M.; Kowarik, S.; Gerlach, A.; Schreiber, F. *Phys. Rev. B* **2008**, *78*, 085210.
(34) Dürr, A. C.; Schreiber, F.; Ritley, K. A.; Kruppa, V.; Krug, J.; Dosch, H.; Struth, B. *Phys. Rev. Lett.* **2003**, *90*, 016104.
(35) Heinrich, M. A.; Pflaum, J.; Tripathi, A. K.; Frey, W.; Steigerwald, M. L.; Siegrist, T. *J. Phys. Chem. C* **2007**, *111*, 18878.
(36) Kowarik, S.; Gerlach, A.; Sellner, S.; Schreiber, F.; Cavalcanti, L.; Konovalov, O. *Phys. Rev. Lett.* **2006**, *96*, 125504.
(37) Scholz, R.; Gisslen, L.; Schuster, B.-E.; Casu, M. B.; Chassé, T.; Heinemeyer, U.; Schreiber, F. *J. Chem. Phys.* **2011**, *134*, 014504.
(38) Wagner, J.; Gruber, M.; Hinderhofer, A.; Wilke, A.; Bröker, B.; Frisch, J.; Amsalem, P.; Vollmer, A.; Opitz, A.; Koch, N.; Schreiber, F.; Brütting, W. *Adv. Funct. Mater.* **2010**, *20*, 4295.
(39) Wagner, J.; Gruber, M.; Wilke, A.; Tanaka, Y.; Topczak, K.; Steindamm, A.; Hörmann, U.; Opitz, A.; Nakayama, Y.; Ishii, H.; Pflaum, J.; Koch, N.; Brütting, W. *J. Appl. Phys.* **2012**, *111*, 054509.
(40) Kurrle, D.; Pflaum, J. *Appl. Phys. Lett.* **2008**, *92*, 133306.
(41) Lunt, R. R.; Giebink, N. C.; Belak, A. A.; Benziger, J. B.; Forrest, S. R. *J. Appl. Phys.* **2009**, *105*, 053711.
(42) Hörmann, U.; Wagner, J.; Gruber, M.; Opitz, A.; Brütting, W. *Phys. Status Solidi RRL* **2011**, *5*, 241−243.
(43) Wilke, A.; Amsalem, P.; Frisch, J.; Bröker, B.; Vollmer, A.; Koch, N. *Appl. Phys. Lett.* **2011**, *98*, 123304.
(44) Smilgies, D.-M.; Boudet, N.; Struth, B.; Konovalov, O. *J. Synchrotron Radiat.* **2005**, *12*, 329−339.
(45) Nelson, A. *J. Appl. Crystallogr.* **2006**, *39*, 273−276.
(46) Birkholz, M. *Thin Film Analysis by X-Ray Scattering*; Wiley-VCH: Weinheim, Germany, 2006.
(47) Hosokai, T.; Horie, M.; Aoki, T.; Nagamatsu, S.; Kera, S.; Okudaira, K. K.; Ueno, N. *J. Phys. Chem. C* **2008**, *112*, 4643−4648.
(48) de Boer, J. L.; van Smaalen, S.; Petricek, V.; Dusek, M.; Verheijen, M. A.; Meijer, G. *Chem. Phys. Lett.* **1994**, *219*, 469−472.
(49) Kowarik, S.; Gerlach, A.; Sellner, S.; Cavalcanti, L.; Konovalov, O.; Schreiber, F. *Appl. Phys. A: Mater. Sci. Process.* **2009**, *95*, 233−239.
(50) Zhang, X.; Barrena, E.; Goswami, D.; de Oteyza, D. G.; Weis, C.; Dosch, H. *Phys. Rev. Lett.* **2009**, *103*, 136101.
(51) Lof, R. W.; van Veenendaal, M. A.; Koopmans, B.; Jonkman, H. T.; Sawatzky, G. A. *Phys. Rev. Lett.* **1992**, *68*, 3924−3927.
(52) Krause, S. *Determination of the transport levels in thin films of organic semiconductors*. Ph.D. Thesis, Universität Würzburg, 2008.
(53) Weaver, J. H.; Martins, J. L.; Komeda, T.; Chen, Y.; Ohno, T. R.; Kroll, G. H.; Troullier, N.; Haufler, R. E.; Smalley, R. E. *Phys. Rev. Lett.* **1991**, *66*, 1741−1744.
(54) Hasegawa, S.; Miyamae, T.; Yakushi, K.; Inokuchi, H.; Seki, K.; Ueno, N. *Phys. Rev. B* **1998**, *58*, 4927−4933.
(55) Molodtsova, O. V.; Knupfer, M. *J. Appl. Phys.* **2006**, *99*, 053704.
(56) Liebsch, T.; Plotzke, O.; Heiser, F.; Hergenhahn, U.; Hemmers, O.; Wehlitz, R.; Viefhaus, J.; Langer, B.; Whitfield, S. B.; Becker, U. *Phys. Rev. A* **1995**, *52*, 457−464.
(57) Duhm, S.; Heimel, G.; Salzmann, I.; Glowatzki, H.; Johnson, R. L.; Vollmer, A.; Rabe, J. P.; Koch, N. *Nat. Mater.* **2008**, *7*, 326−332.
(58) Fukagawa, H.; Yamane, H.; Kataoka, T.; Kera, S.; Nakamura, M.; Kudo, K.; Ueno, N. *Phys. Rev. B* **2006**, *73*, 245310.
(59) Hinderhofer, A.; Hosokai, T.; Yonezawa, K.; Gerlach, A.; Kato, K.; Broch, K.; Frank, C.; Novak, J.; Kera, S.; Ueno, N.; Schreiber, F. *Appl. Phys. Lett.* **2012**, *101*, 033307.
(60) Ueno, N.; Kera, S. *Prog. Surf. Sci.* **2008**, *83*, 490−557.
(61) Kera, S.; Yamane, H.; Ueno, N. *Prog. Surf. Sci.* **2009**, *84*, 135−154.
(62) He, P.; Bao, S.; Yu, C.; Xu, Y. *Surf. Sci.* **1995**, *328*, 287−290.
(63) Tycko, R.; Dabbagh, G.; Fleming, R. M.; Haddon, R. C.; Makhija, A. V.; Zahurak, S. M. *Phys. Rev. Lett.* **1991**, *67*, 1886−1889.
(64) Fukagawa, H.; Kera, S.; Kataoka, T.; Hosoumi, S.; Watanabe, Y.; Kudo, K.; Ueno, N. *Adv. Mater.* **2007**, *19*, 665−668.
(65) Mao, H. Y.; Bussolotti, F.; Qi, D.-C.; Wang, R.; Kera, S.; Ueno, N.; Wee, A. T. S.; Chen, W. *Org. Electron.* **2011**, *12*, 534−540.
(66) Greiner, M. T.; Helander, M. G.; Tang, W.-M.; Wang, Z.-B.; Qiu, J.; Lu, Z.-H. *Nat. Mater.* **2012**, *11*, 76−81.
(67) Braun, S.; Salaneck, W. R.; Fahlman, M. *Adv. Mater.* **2009**, *21*, 1450−1472.
(68) Vazquez, H.; Gao, W.; Flores, F.; Kahn, A. *Phys. Rev. B* **2005**, *71*, 041306.
(69) Linares, M.; Beljonne, D.; Cornil, J.; Lancaster, K.; Brédas, J.-L.; Verlaak, S.; Mityashin, A.; Heremans, P.; Fuchs, A.; Lennartz, C.; Idé, J.; Méreau, R.; Aurel, P.; Ducasse, L.; Castet, F. *J. Phys. Chem. C* **2010**, *114*, 3215−3224.
(70) Ivanco, J. *Thin Solid Films* **2012**, *520*, 3975−3986.